ARTICLE

Human Osteoclast-Poor Osteopetrosis with Hypogammaglobulinemia due to *TNFRSF11A* (*RANK*) Mutations

Matteo M. Guerrini,[1,2] Cristina Sobacchi,[1,2] Barbara Cassani,[2] Mario Abinun,[3] Sara S. Kilic,[4] Alessandra Pangrazio,[1,2] Daniele Moratto,[5] Evelina Mazzolari,[5] Jill Clayton-Smith,[6] Paul Orchard,[7] Fraser P. Coxon,[8] Miep H. Helfrich,[8] Julie C. Crockett,[8] David Mellis,[8] Ashok Vellodi,[9] Ilhan Tezcan,[10] Luigi D. Notarangelo,[5,11] Michael J. Rogers,[8] Paolo Vezzoni,[1,2] Anna Villa,[1,2,12,*] and Annalisa Frattini[1,2]

Autosomal-Recessive Osteopetrosis (ARO) comprises a heterogeneous group of bone diseases for which mutations in five genes are known as causative. Most ARO are classified as osteoclast-rich, but recently a subset of osteoclast-poor ARO has been recognized as due to a defect in *TNFSF11* (also called *RANKL* or *TRANCE,* coding for the RANKL protein), a master gene driving osteoclast differentiation along the RANKL-RANK axis. RANKL and RANK (coded for by the *TNFRSF11A* gene) also play a role in the immune system, which raises the possibility that defects in this pathway might cause osteopetrosis with immunodeficiency. From a large series of ARO patients we selected a Turkish consanguineous family with two siblings affected by ARO and hypogammaglobulinemia with no defects in known osteopetrosis genes. Sequencing of genes involved in the RANKL downstream pathway identified a homozygous mutation in the *TNFRSF11A* gene in both siblings. Their monocytes failed to differentiate in vitro into osteoclasts upon exposure to M-CSF and RANKL, in keeping with an osteoclast-intrinsic defect. Immunological analysis showed that their hypogammaglobulinemia was associated with impairment in immunoglobulin-secreting B cells. Investigation of other patients revealed a defect in both *TNFRSF11A* alleles in six additional, unrelated families. Our results indicate that *TNFRSF11A* mutations can cause a clinical condition in which severe ARO is associated with an immunoglobulin-production defect.

Introduction

Autosomal-recessive osteopetrosis (ARO) in humans represents a heterogeneous group of diseases, including osteoclast-rich and osteoclast-poor forms.[1] The osteoclast-rich form, characterized by a normal or even elevated number of nonfunctional multinucleated osteoclasts, is due to defects in genes involved in the bone-resorbing function of osteoclasts.[2–5] The osteoclast-poor form, in which no mature osteoclasts are present, has remained poorly understood until recently, when our group identified *TNFSF11* (MIM 602642) mutations in some patients (3% in our cohort).[6] A very rare form of osteopetrosis with anhydrotic ectodermal dysplasia and immunodeficiency (MIM 300291), due to mutation of the *IKBKG* gene (NEMO, [MIM 300248]), has also been reported.[7]

RANKL, the protein coded for by the *TNFSF11* gene, binds to two different receptors: the membrane-anchored receptor RANK, coded by the *TNFRSF11A* gene (MIM 603499), and the soluble decoy receptor osteoprotegerin (OPG), coded by the *TNFRSF11B* gene (MIM 602643). RANKL signaling through RANK is fundamental for osteoclast maturation, as demonstrated by osteopetrosis in mice due to targeted deletion of either gene. In fact, *Tnfrsf11a*$^{-/-}$ (*rank* knockout)[8] and *Tnfsf11*$^{-/-}$ (*rankl* knockout)[9–11] mice share a similar phenotype, with severe osteopetrosis due to complete lack of mature osteoclasts, immune deficiency with absent lymph nodes, defective mammary-gland maturation, and other minor abnormalities. Monocytes from both *Tnfsf11*$^{-/-}$ mice and ARO patients bearing mutations in *TNFSF11* differentiate normally when exposed to recombinant RANKL, confirming that the defect is outside the osteoclast lineage.[6,9] By contrast, the osteoclast differentiation defect of *Tnfrsf11a*$^{-/-}$ mice cannot be rescued by exogenous RANKL.[8]

Therefore, we analyzed genes involved in osteoclast differentiation along the RANKL-RANK axis in other osteoclast-poor individuals without *TNFSF11* mutations. Here, we report seven mutations in the *TNFRSF11A* gene leading to an osteoclast-poor ARO phenotype due to a cell-autonomous defect in eight patients. Importantly, as opposed to *TNFSF11* deficiency, osteopetrosis in *TNFRSF11A*-deficient patients could be rescued by hematopoietic stem cell transplantation (HSCT). Overall, these findings

[1]Istituto di Tecnologie Biomediche, Consiglio Nazionale delle Ricerche, Segrate 20090, Italy; [2]Istituto Clinico Humanitas IRCCS, Rozzano 20089, Italy; [3]Children's BMT Unit, Newcastle General Hospital and Newcastle University, Newcastle upon Tyne NE4 6BE, UK; [4]Department of Pediatric Immunology, Faculty of Medicine, Uludag University, Bursa 16200, Turkey; [5]Centro di Trapianto di Midollo Osseo e Istituto di Medicina Molecolare "Angelo Nocivelli," Clinica Pediatrica, Università di Brescia, Brescia 25100, Italy; [6]Department of Clinical Genetics, St. Mary's Hospital, Manchester, M13 9WL, UK; [7]Program in Blood and Marrow Transplantation, Department of Pediatrics, University of Minnesota, Minneapolis, MN 55455, USA; [8]Bone & Musculoskeletal Programme, School of Medicine and Dentistry, Institute of Medical Sciences, University of Aberdeen, Aberdeen AB25 2ZD, UK; [9]Great Ormond Street Children's Hospital NHS Trust, London WC1N 3JH, UK; [10]Hacettepe University, Children's Hospital, Pediatric Immunology Unit, Ankara 06100, Turkey; [11]Division of Immunology, Children's Hospital, Harvard Medical School, Boston, MA 02115, USA; [12]San Raffaele Telethon Institute for Gene Therapy (HSR-TIGET), Milan 20132, Italy
*Correspondence: anna.villa@itb.cnr.it
DOI 10.1016/j.ajhg.2008.06.015.

demonstrate that even among patients with a similar phenotype (e.g., osteoclast-poor ARO), careful genetic diagnosis has significant prognostic and therapeutic implications.

Material and Methods

Analysis of In Vitro Osteoclast Function

Human osteoclasts were generated by culture of peripheral blood monocytes with M-CSF and RANKL as previously described,[12] with minor modifications. PBMCs were isolated from 10 ml of peripheral blood from the patients or an unrelated control and cultured in α-MEM with 20 ng/ml M-CSF (R&D Systems) for 7 days, with a complete change of medium after 4 days. The M-CSF-dependent macrophages were rinsed in PBS and then scraped into fresh medium after incubation for 15 min in 1 mg/ml trypsin. After cells were centrifuged and resuspended in fresh medium, they were seeded on to 9 mm glass coverslips in 48-well plates or 5 mm discs of dentine in 96-well plates (6×10^4 and 2×10^4 cells/well, respectively) and incubated with 20 ng/ml M-CSF and 100 ng/ml RANKL (Peprotech) for 10 days, with complete media changes after 3 and 6 days. Cells were then fixed in either paraformaldehyde (for light-microscopic analysis) or in glutaraldehyde (for electron-microscopic analysis) as described previously.[6] For light microscopy, osteoclasts were immunostained for the vitronectin receptor (VNR; antibody courtesy of Mike Horton, University College London), and acidic vesicles, F-actin, nuclei and the dentine surface were visualized as previously described.[6] Cells were analyzed by the use of confocal microscopy with a Zeiss LSM 510 confocal microscope equipped with argon (excitation 488 nm) and helium-neon (543 nm and 633 nm) lasers. Osteoclast formation was quantified in cultures from patient 1A (Pt. 1A), Pt 6, Pt 7, and appropriate controls by a count of the number of VNR-positive cells with more than two nuclei (replicates of at least four). For scanning electron microscopy, osteoclast cultures were processed as previously described[6] and then examined in a Jeol 35S scanning electron microscope at 10 kV. Images were taken with SemAfore software.

Bone Biopsies

Bone biopsies were taken from the iliac crest. Tissue was fixed in formalin, demineralized in EDTA, and embedded in paraffin according to standard procedures. Sections were stained with hematoxylin and eosin or with toluidine blue. In one case (Pt. 5), sections were also stained for expression of tartrate-resistant acid phosphatase (TRAcP), with napthol-ASBI-phosphate used as substrate and pararosanilin used as coupler, and counterstained with hematoxylin. Sections were analyzed with a Zeiss Axioskop 40 microscope and photographed with a Progress camera.

Mutation Analysis

Specimens, including frozen peripheral-blood cells, EBV-transformed lymphoblast cell lines, and DNA samples, were collected from patients after their parents provided informed consent. The study was approved by the National Research Council. *TNFRSF11A* gene (transcript ID number NM_003839) analysis was performed by PCR amplification with the primers reported in Table S1 (available online). All of the reactions were performed in 25 μl of final volume with 0.4 U Taq polymerase, 1.5 mM $MgCl_2$, 300 μM dNTPs, 10 pmol of each oligonucleotide primer, and 20 ng of purified genomic DNA. The thermocycling conditions used for amplification consisted of an initial denaturation step at 94°C for 3 min, followed by 34 cycles of denaturation at 94°C for 30 s and annealing at 60°C for 30 s and 72°C for 30 s. The amplification of exons 1 and 11 was performed with the PCRx Enhancer System (Invitrogen). Automated sequencing was performed directly on the PCR products purified from the gel.

Western-Blot Analysis of RANK Signaling

M-CSF-dependent peripheral-blood monocytes from Pt. 1A or a healthy volunteer were cultured in 12-well tissue-culture plates (2×10^5 cells/well) in α-MEM + 10% fetal-calf serum + 10 ng/ml recombinant human M-CSF (R&D Systems). The cells were starved of serum and M-CSF for 2 hr and then treated with 100 ng/ml recombinant human RANKL or 10 ng/ml TNFα (Peprotech) for 10 or 15 min. Cells were then lysed in 50 μl buffer containing 10 mM potassium phosphate pH 7.4, 137 mM NaCl, 0.1% (w/v) SDS, 0.5% (w/v) sodium deoxycholate, 1% (v/v) Triton X-100, 1mM EDTA, and protease and phosphatase inhibitors. Lysates were cleared and assayed for protein with the use of the BCA assay (Pierce). Fifty micrograms of protein from each sample were then resolved by SDS-PAGE on 12% polyacrylamide-SDS gels followed by transfer onto PVDF membranes and simultaneous hybridization with anti-phospho p38 and total p38 antibodies or with anti-phospho ERK1/2 and total ERK1/2 antibodies (Cell Signaling). Bands were detected on a Li-Cor Odyssey imager after the blots were incubated with Alexafluor680- and IRDye800-conjugated secondary antibodies (Molecular Probes and Rockland Immunochemicals, respectively).

Flow-Cytometry Analysis

The percentage of T cells, B cells, and myeloid cells in the peripheral blood was assessed by the use of flow cytometry. Fresh peripheral-blood cells (2×10^5 cells), erythrocyte-depleted, were preincubated for 15 min at RT with mouse serum and stained for 20 min at 4°C with the following mouse anti-human monoclonal antibodies, from BD PharMingen or Caltag Laboratories, either FITC, PE, perCp or APC/conjugated: anti-CD3, anti-CD4, anti-CD8, anti-CD14, anti-CD19, anti-CD20, anti-CD21, anti-CD27, anti-CD38, anti-CD45RO, anti-CD80, anti-CD86, anti-CCR7, anti-IgD. After washing, cells were acquired on a FACScalibur flow cytometer and analyzed with FlowJo (version 4.5.4; Treestar) and FCSexpress (version 3.0) software.

Lymphocyte Proliferation

Peripheral-blood mononuclear cells (PBMCs) were purified from peripheral blood by centrifuge separation on Lymphoprep (Nycomed Pharma AS) and suspended in RPMI 1640 containing 10% FBS, 1% penicillin/streptomycin, 4 μM glutamine. For T cell proliferation, 10^5 cells per well were placed in a round-bottom 96-well plate in the presence of human PMA (40 ng/ml) and Ionomycin (100 ng/ml) or with anti-CD3 antibodies (2 μg/ml) (BD PharMingen) alone or combined with either anti-CD28 antibody (5 μg/ml) (BD PharMingen) or IL-2 (100 U/ml) (Proleukin-Chiron). T cell proliferation was analyzed after 72 hr of stimulation by the use of a 16 hr pulse with 1 μ Ci/well ^{3}[H] thymidine (Amersham Biosciences) followed by harvesting and counting via liquid scintillation. All the experiments were performed in triplicate.

Monocyte-Derived Dendritic Cell Preparation

In brief, highly enriched monocytes were obtained from peripheral blood by Lymphoprep (Nycomed Pharma AS) gradient

centrifugation followed by $CD14^+$ cell selection by immunomagnetic beads (Miltenyi). Monocytes were cultured for 6 days at 10^6/ml in 6-well tissue-culture plates (Falcon; BD Biosciences) in RPMI 1640 supplemented with 10% FCS, 50 ng/ml GM-CSF, and 20 ng/ml IL-4. Dendritic cell (DC) maturation was driven by additional 24 hr culture in the presence of 200 ng/ml LPS.

Mixed-Leukocyte Reaction

5×10^4 immature or LPS-stimulated DCs were added to 5×10^5 $CD45RA^+$-enriched allogeneic T cells in 96-well plates. Each analysis was performed in triplicate. Cell proliferation was analyzed at day 4 of stimulation by a 16 hr pulse with 1 μ Ci/well ^{3}[H] thymidine (Amersham Biosciences) followed by harvesting and counting by liquid scintillation.

Results

Clinical Evaluation of Patients

Here, we report eight patients from seven unrelated families, found to have mutations in *TNFRSF11A*.

Pt. 1A and Pt. 1B were two siblings of Turkish consanguineous parents (Figure 1A, Family 1). The elder (Pt. 1A) was first hospitalized at 2.5 years of age with progressive visual loss, nystagmus, and recurrent pneumonia. Physical examination revealed an enlarged liver and spleen and increased head circumference (>98th percentile). A CT scan of the head showed enlarged lateral ventricles and severe narrowing of the optic foramina. A blood count revealed moderate anemia and thrombocytopenia. Immunological investigation showed hypogammaglobulinemia and lack of antibody response to tetanus antigen (0.005 IU/ml). Peripheral-blood T and B cell absolute counts were normal (data not shown). The patient was started on regular intravenous immunoglobulin infusions (IVIG) (400 mg/kg, every 3 weeks). Prednisolone (5 mg/m^2/day) and calcitriol (0.5 mg/day) were given for 6 months. HSCT was not performed due to lack of an HLA-matched donor. Bone hypertrophy in the nasal cavity caused a protracted suffocation episode at the age of 5 years, which required tracheostomy. However, irreversible CNS damage ensued, leading to a permanent vegetative state.

Her brother, Pt. 1B, was diagnosed with osteopetrosis at 4 months. He had severe visual impairment, nystagmus, hypotonia, and motor and mental retardation. Neither fractures nor bone-marrow failure was observed. VEP and BERA revealed slow stimuli transmission in anterior visual pathways and bilateral peripheral and bulbopontine auditory pathways, respectively. In addition, he suffered from recurrent respiratory infections. X-rays documented a generalized increase in density consistent with the diagnosis of osteopetrosis (Figure 2A, left). Hypogammaglobulinemia was diagnosed, and treatment with IVIG was given, albeit irregularly. The child died of pneumonia at the age of 3 years.

Pt. 2, of Argentinean origin, has previously been described[13] (Figure 1A, Family 2). At 45 days of age, abnormal eye movements were noticed. Increased bone density was documented at 3.5 months, and a diagnosis of osteopetrosis was established. At that time, moderate anemia (Hb 9.1 g/dL) was present. Bone-marrow biopsy showed decreased cellularity, with reduced hematopoiesis and lack of osteoclasts. Brain MRI was normal and the patient had good development of social skills, but gross motor milestones were delayed. The infant received a 4/6 HLA antigen-matched unrelated-cord-blood transplant at 8 months of age, with a preparative regimen consisting of busulfan (8 mg/kg), fludarabine (175 mg/m^2), antithymocyte globulin (ATG horse; 150 mg/kg) and total-lymphocyte irradiation (TLI 500 cGy). Initial engraftment was followed by loss of the graft by day +100. The patient died of respiratory arrest at less than one year after transplant. Post mortem examination was not performed.

Pt. 3 was the third child of unrelated Caucasian parents (Figure 1A, Family 3). He presented during the first week of life with hypocalcemic seizures, which responded to calcium and vitamin D. He was hospitalized again, at 6 weeks and at 2 months of age, with respiratory infections. A diagnosis of ARO was made at 3 months, when he was noticed to have no eye contact and was not smiling. He had bilateral optic-nerve atrophy; visual evoked responses were delayed and abnormal, consistent with marked optic nerve compression. He was pale, with mild hepatosplenomegaly, and was not gaining weight normally. Skeletal radiography revealed multiple rib fractures and dense bones (Figure 2A, right). He suffered several episodes of cardiac/respiratory arrest due to hypocalcemia and respiratory infections and was started on interferon-gamma treatment. At 5 months of age, a bone biopsy (Figure 2E) showed increase of bony and cartilaginous trabeculae, narrowing of marrow space, and very few osteoclasts. Immunological investigation revealed hypogammaglobulinaemia and lack of antibody response to tetanus toxoid (Table 1), with normal peripheral blood T and B lymphocyte absolute numbers (data not shown). HSCT was performed from a 7/8 HLA-antigen-matched unrelated donor at 7 months, after myeloablative conditioning with busulfan (16 mg/kg) and cyclophosphamide (200 mg/kg) with Campath 1G from day −4 to day +4. A total dose of 1.5×10^9/kg bone-marrow nucleated cells were infused. Cyclosporin A was used for prophylaxis of graft-versus-host disease (GvHD). At the time of very early signs of engraftment, on day +15 he developed severe hepatic veno-occlusive disease (VOD), followed by pneumonitis on day +19, progressing to multi-organ system failure and death on day +22. Autopsy confirmed acute respiratory distress syndrome (ARDS) and severe liver VOD as causes of death, as well as atrophy of optic and olfactory nerves due to bone compression and engraftment with evidence of hemopoiesis and osteoclast activity.

Pt. 4 is the first child born to first-cousin Pakistani parents (Figure 1A, Family 4). At 7 days, he developed hypocalcemic seizures. Poor visual fixation and roving nystagmus were noticed at 6.5 months, and optic-nerve atrophy was demonstrated with an MRI scan. A hand radiograph showed alternating bands of radio density and lucency at the

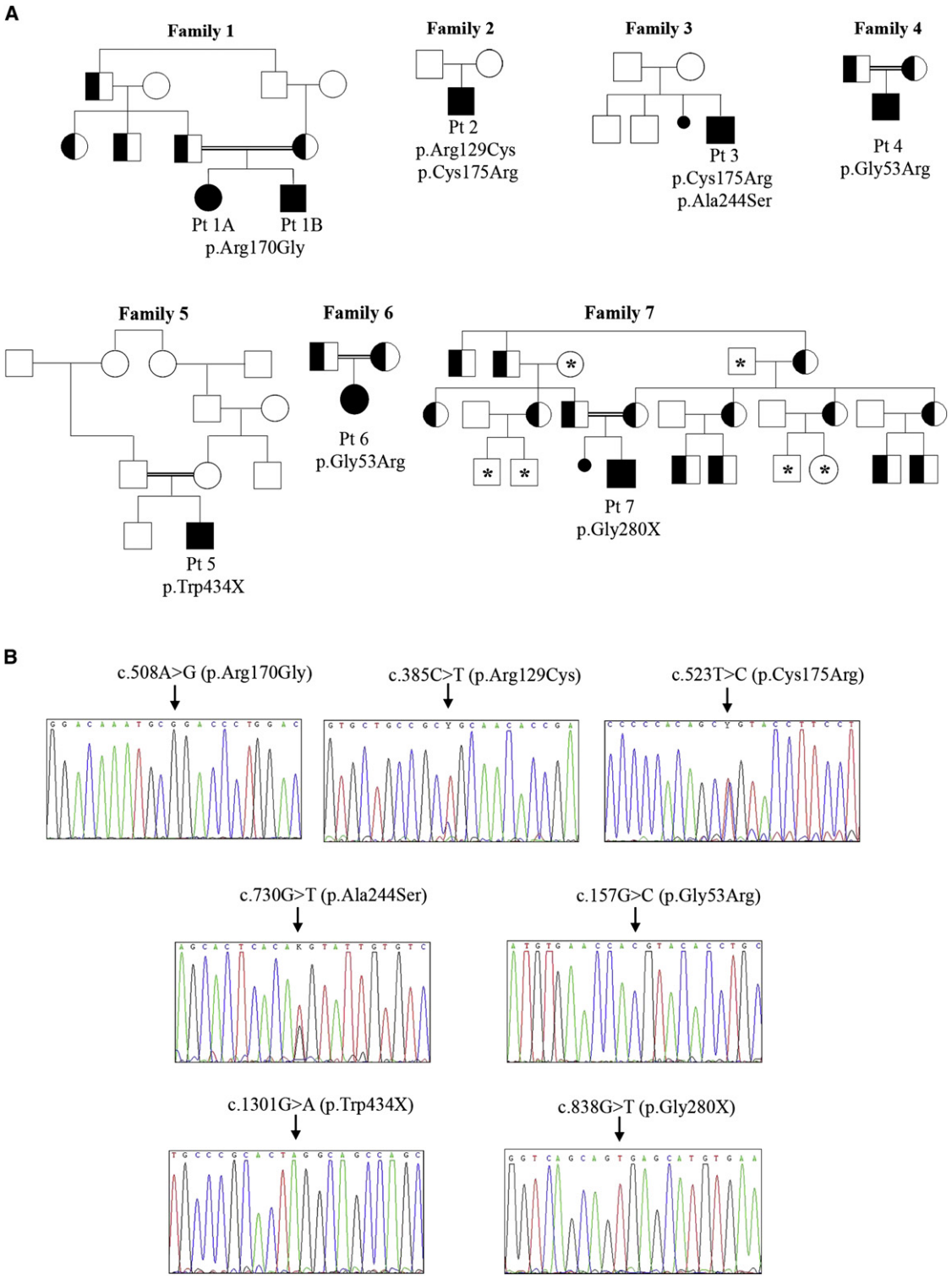

Figure 1. Pedigree of the Affected Patients and Mutation Analysis

(A) Pedigrees of the seven analyzed families. Black circles or squares in the pedigrees indicate affected members with both mutated alleles. Half-black circles or squares indicate heterozygous members with only one mutated allele. White symbols indicate members not analyzed, except those with asterisks in Family 7, which have been analyzed and are normal. Below each pedigree, the amino acid change(s) is indicated.

(B) Chromatograms of the seven mutations in the *TNFRSF11A* gene are indicated.

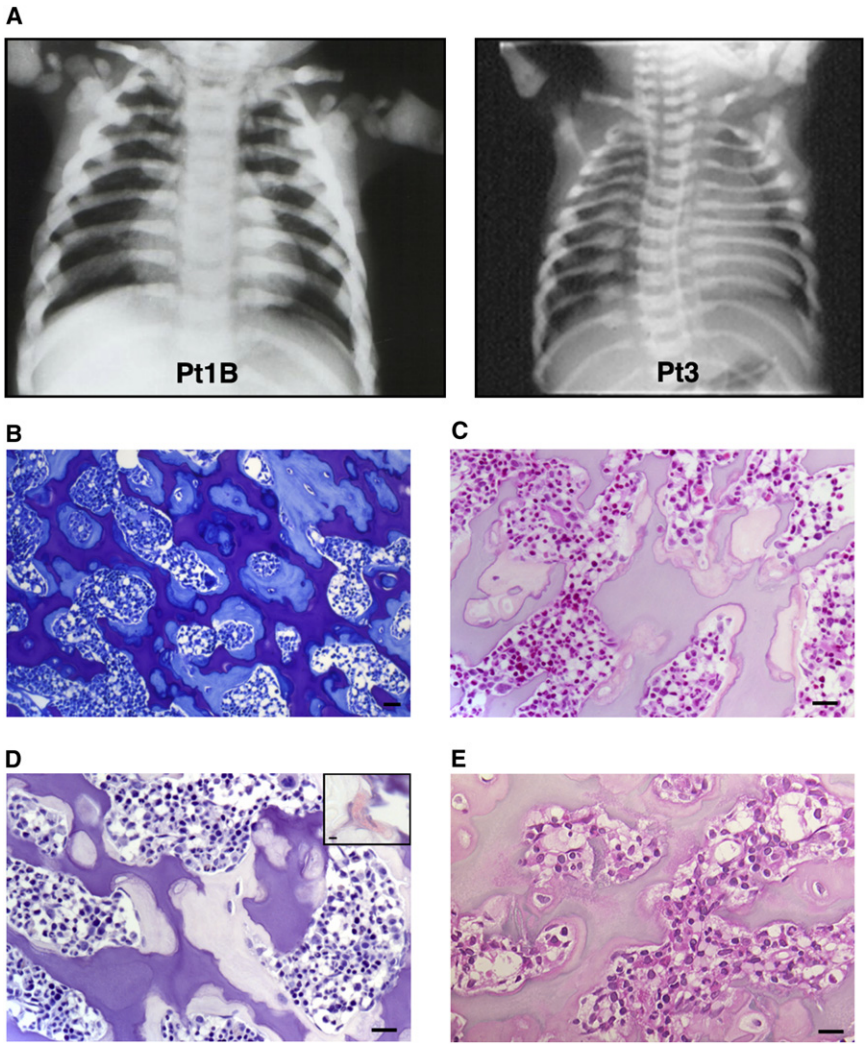

Figure 2. Chest X-Rays and Bone Biopsies of Some Patients

(A) Bone thickening of vertebrae and ribs is evident, revealing classical osteopetrotic phenotype in Pt. 1B and Pt. 3. Panels B–D show bone biopsies from Pt. 5, panel E from Pt. 3.

(B) Toluidine-blue staining: dark purple indicates cartilage, blue indicates bone.

(C) Hematoxylin-eosin staining: abundant hematopoietic cells in the scarce marrow spaces; cartilage is shown in gray and bone in pink. There are neither multinucleated cells nor active osteoblasts.

(D) TRAcP staining, counterstained with hematoxylin. No TRAcP positive cells are present; the inset shows a control section with a TRAcP-positive osteoclast for comparison.

(E) Section of bone from Pt. 3 stained with hematoxylin and eosin, illustrating abundance of trabecular bone (pink) and cartilage (gray), absence of multinucleated cells, and absence of active bone formation.

Scale bar represents 50 μm in panels B–E. Scale bar in panel D represents 10 μm.

metaphyses and increased bone density of the diaphyses, thus confirming the diagnosis of osteopetrosis. The liver was palpable 2 cm below the costal margin, but no significant hematological abnormalities were present. HSCT was performed, with the patient's HLA-identical mother as donor. Full engraftment was associated with resolution of radiological features of osteopetrosis. However, feeding difficulties, developmental delay, and lack of vision have persisted. At two years of age, the patient shows a lack of speech development.

Pt. 5 is the second child of a consanguineous Caucasian couple (Figure 1A, Family 5). He presented at 3 days of life with afebrile seizures, which required prolonged treatment with phenobarbital. A CT scan of the brain showed multiple hematomas. At 2 months of age, the infant was noticed to have no eye contact. Visual evoked responses were delayed and abnormal. Skeleton X-ray examination was compatible with osteopetrosis. The patient was referred for HSCT at 8 months of age. At that time, severe developmental delay, growth failure (weight and length $< 3^{rd}$ percentile), and nystagmus were present. There were no signs of liver or spleen enlargement. A bone-marrow biopsy (Figures 2B–2D) showed thickened trabecular bone with reduced lacunae and presence of normal hematopoietic lines. No signs of osteoclast activity were documented. The infant developed recurrent seizures, with myoclonic twitches and irregular theta waves admixed with high-frequency activity at EEG tracing. Immunological evaluation revealed normal serum immunoglobulins (Table 1). HSCT was performed from an HLA-identical sibling at 1 year of age, after myeloablative conditioning with busulfan (20 mg/kg), thiotepa (5 mg/kg) and cyclophosphamide (200 mg/kg). A total of 0.35×10^9/kg bone-marrow nucleated cells, containing 4.9×10^6/kg $CD34^+$ cells, were infused. Cyclosporin A was used for prophylaxis of GvHD. Full donor engraftment was achieved. At 3 years after transplantation, the patient has normal hematopoiesis, with correction of radiological signs of osteopetrosis. Progressive improvement of EEG tracing has been recorded, allowing for gradual tapering of anticonvulsants.

Pt. 6 was born from consanguineous Pakistani parents (Figure 1A, Family 6); there appeared to be no relationship between this family and the family of Pt. 4. She was diagnosed at 9 months of age, when she presented with hydrocephalus. She was also Bilevel Positive Airway Pressure (BiPAP)-dependent. Routine X-rays done at that time showed features of ARO and a fracture of the left femur. Vision was normal at presentation, but progressive visual loss developed, and focal narrowing of optic nerves was revealed by MRI. No hepatosplenomegaly was reported. EMG

Table 1. Clinical and Laboratory Features

Clinical Data[a]	Pt. 1A	Pt. 1B	Pt. 2	Pt. 3	Pt. 4	Pt. 5	Pt. 6	Pt. 7
Age at onset/diagnosis	3 months/2.5 years	1 month/4 months	2 months/3.5 months	1 week/3 months	1 week/6 months	1 week/2 months	9 months/ 9 months	2 months/ 8 months
Bone biopsy (pre-HSCT[c])	nd	nd	few/no osteoclasts, significant reduction of medullary space	few/no osteoclasts, significant reduction of medullary space	nd	few/no osteoclasts, significant reduction of medullary space	nd	nd
Bone fractures	no	no	no	multiple ribs	no	no	left femur	yes
Neurological defects	severe visual impairment, nystagmus, enlarged lateral ventricles, severe motor and mental retardation	severe visual impairment, nystagmus, hypotonia, severe motor and mental retardation	visual impairment, nystagmus, delayed gross motor milestones	visual impairment, mild hearing loss, hypocalcemic spasms, mild developmental delay	visual impairment, neurodevelopmental delay, hypocalcemic seizures	visual impairment, nystagmus, seizures, developmental delay	visual impairment, hydrocephalus motor abnormalities	visual impairment
Hepatospleno-megaly	yes	no	no	yes	mild hepatomegaly	no	no	mild hepatospleno-megaly
Other features	recurrent pneumonia	recurrent upper respiratory tract infections	none	respiratory infections growth failure	none	growth failure	BiPAP[b] ventilation	growth failure
Hb[d] (g/dl)	10.0	8.7	9.1	10.5	10.0	10.4	9.8	8.9
Plt[e] ($\times 10^9$/L)	150	191	170	346	223	334	nd	263
WBC[f] ($\times 10^9$/L)	15.2	11.9	33.5	9.4	9.8	11.4	10.5	12.2
Neutrophils (% of WBC[f])	42	37	nd	14	25	41.6	50	50
Lymphocytes (% of WBC[f])	56	57	nd	73	60	47.1	40	48
Monocytes (% of WBC[f])	2	6	nd	10	5	nd	10	2
Immunoglobulin G (mg/dl)	435 (604–1941)	354 (605–1430)	nd	144 (230–850)	nd	502 (172–1069)	nd	nd
Immunoglobulin M (mg/dl)	45.1 (71–235)	18 (66–228)	nd	19 (19–86)	nd	66 (41–173)	nd	nd
Immunoglobulin A (mg/dl)	22.5 (26–296)	29 (30–107)	nd	33 (10–50)	nd	76 (11–106)	nd	nd
Tetanus vaccination (IU/ml)	0.005		nd	< 0.08 (> 0.1)	nd	nd	nd	nd
Age at HSCT[c]	not performed	not performed	8 months	7 months	6 months	1 year	not performed	not performed
HSC[g] origin			umbilical cord blood unrelated	bone marrow unrelated	bone marrow HLA-id parent	bone marrow HLA-id sibling		
Donor								
T cell depletion (TCD)	-	-	no TCD	no TCD	no TCD	no TCD	-	-
Engraftment (% donor chimerism)	-	-	graft loss day +100	osteoclast activity (post mortem)	100%	100% (in all blood lineages)	-	-
Bone remodeling	-	-	n/a	n/a	yes (X-ray)	yes (X-ray)	-	-
Outcome	alive at 7 years	died at 3 years	died $<$ 1 yr post-HSCT	died day +22 post-HSCT	alive at 5 years	alive at 4.5 years	alive at 2 years	alive at 5 years

nd: not done; n/a: not assessed.

Normal values for 1-year-old children: WBC = 6–17.5; Hb = 10.5–12.0; Plt = 150–400.

[a] All of the laboratory data reported refer to the time of the first diagnosis.

[b] BiPAP: Bilevel Positive Airway Pressure.

[c] HSCT: Haematopoietic Stem Cell Transplantation.

[d] Hb: Hemoglobin.

[e] Plt: Platelets.

[f] WBC: White Blood Cells.

[g] HSC: Haematopoietic Stem Cells.

revealed chronic denervation and reinnervation in both bulbar and limb musculature. Foramen magnum decompression was performed as a result of the restriction of posterior fossa and foramen magnum, with consequent cerebellar peduncles towering. The patient has not yet been transplanted and is alive at 2 years of age.

Pt. 7 is the first child of consanguineous Turkish parents (Figure 1A, Family 7). When he was 2 months old, abnormal eye movement was observed by his family. He had a bone fracture at 8 months. X-ray suggested a diagnosis of ARO, and the patient was referred to Hacettepe Children's Hospital. At admission, he was 9 months old, with a weight of 7 kg (3^{rd}–10^{th} percentile) and a height of 68 cm (25^{th} percentile) and mild anemia (Hb: 8.9 g/dL). Light reflex was poor, and mild hepatosplenomegaly was detected. Exophtalmus was prominent. He has no recurrent infection history and is alive at 5 years of age without transplant.

Bone Biopsies

Bone-biopsy specimens were available in three patients. As previously described,[13] extensive trabecular structures, with retention of large areas of cartilage, complete absence of multinucleated cells, and lack of osteoclastic resorption, were present in Pt. 2. Similar findings were observed in bone biopsies from Pt. 3 and Pt. 5 (Figures 2B–2E). Histochemical staining for TRAcP was negative and excluded possible presence of small, mononuclear osteoclasts in the bone biopsy from Pt. 5 (Figure 2D).

Genetic Findings

Among 230 patients with a clinical diagnosis of ARO referred to our institution for genetic investigation, about 28% lack mutations in genes known to cause ARO. Here, we report the identification of mutations in the *TNFRSF11A* gene in seven unrelated families (Figure 1B and Figure 3).

In Family 1, both siblings carried a homozygous transition, c.508A → G, causing a p.Arg170Gly amino acid change in the extracellular domain of RANK, and their parents and several relatives were heterozygous for the nucleotide substitution.

Pt. 2 was a compound heterozygote for two transitions, c.385C → T and c.523T → C, leading to predicted amino acid changes, p.Arg129Cys and c.523T → C, respectively, both in the extracellular domain. The p.Cys175Arg mutation also lies at an exon-intron boundary.

Pt. 3 shared with Pt. 2 the c.523T → C change on one allele, whereas on the other he had a c.730G → T transversion, causing a p.Ala244Ser amino acid substitution in the intracellular domain.

Pt. 4 and Pt. 6 were homozygous for a c.157G → C transversion, causing a p.Gly53Arg amino acid change in the extracellular domain. Both consanguineous parents from both families were heterozygous for the same mutation.

Pt. 5 was homozygous for a c.1301G → A mutation, causing a stop at codon 434 (p.Trp434X) in the intracellular domain.

Pt. 7 was homozygous for a c.838G → T mutation, causing a stop at codon 280 (p.Gly280X) in the intracellular domain. Both consanguineous parents were heterozygous for the mutation. DNA from 18 additional family members, of which 12 were heterozygous, was analyzed.

None of the missense mutations were found in more than 100 chromosomes from healthy unrelated individuals from the same geographical areas. This translates to an 80% power of detecting an SNP with 2% frequency.[14] Sequence alignment of human RANK protein with that of other mammals and chicken showed that the affected residues G53, R129, C175, and A244 are highly conserved throughout evolution, although R170 displays a lower degree of conservation (Figure 3).

Osteoclast Differentiation and Function in Patients from Families 1, 6, and 7

We analyzed the ability of osteoclasts to differentiate in vitro from monocytes isolated from nontransplanted patients (Pt. 1A, Pt. 1B, Pt. 6, Pt. 7), as compared to appropriate controls. Monocytes were induced to differentiate toward the osteoclast lineage by culturing with M-CSF and RANKL.[6,12] Whereas multinucleated, VNR-positive osteoclasts formed readily in cultures from the (unrelated) control, very few osteoclasts formed from either Pt. 1A or Pt. 1B under these conditions (Figure 4A; osteoclast numbers: 2.8 ± 1.7 for Pt. 1A, compared to 61.8 ± 23 for unrelated control; means ± SD of four replicates). Although some VNR-positive cells could be detected, these were mostly mononuclear or binuclear, similar to control cultures with M-CSF alone (data not shown). In cultures of PBMCs from Pt. 6 (data not shown) and Pt. 7 (Figure 4B), osteoclast formation was equally absent, with only small mononuclear VNR-positive cells formed in numbers similar to those seen in cultures with M-CSF alone, whereas in (parent) control cultures, large multinucleated osteoclasts were formed (osteoclast numbers: 4 ± 1.1 for Pt. 6, compared to 324 ± 45 for parent control, and 1.5 ± 0.6 for Pt. 7, compared to 127.3 ± 28 for unrelated control; means ± SD of at least four replicates). Moreover, when cultured on dentine, osteoclasts from the control of Pt. 1A polarized their cytoskeleton into a characteristic F-actin ring and resorbed large pits in the dentine, whereas none of the cells in the patient cultures formed actin rings or showed any evidence of resorptive activity (Figure 4C and Figure S1). Also, mononuclear cells in patient cultures were predominantly spindle-shaped, indicative of defects in the early stages of differentiation toward the osteoclast phenotype (Figure 4 and Figure S1).

Stimulation through the RANKL-RANK axis activates downstream signaling pathways involving phosphorylation of p38.[15] When cultured monocytes were exposed to RANKL, a marked increase in phosphorylated p38 and ERK1/2 was detected in lysates from control cells but not

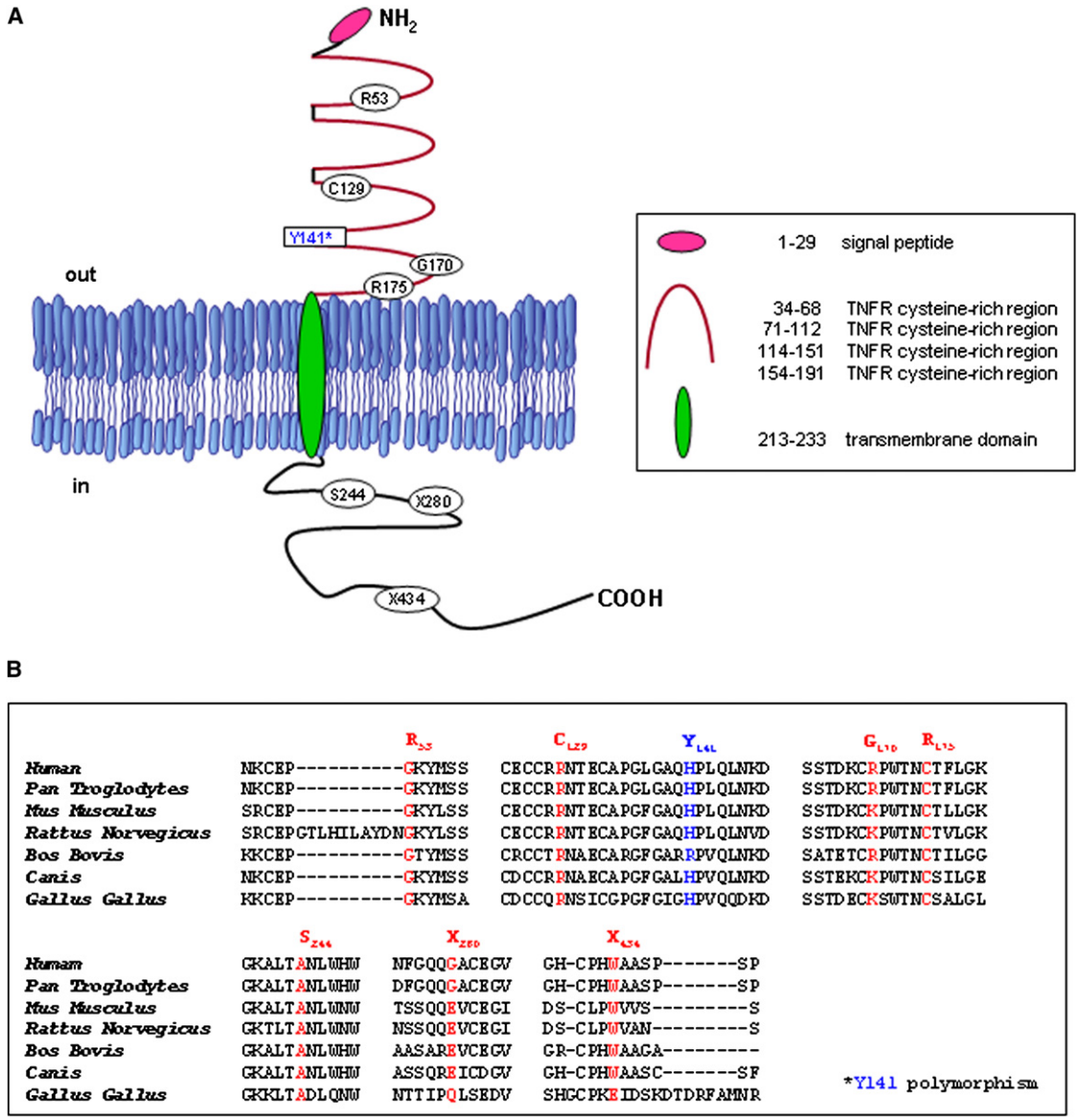

Figure 3. Mutations in Relation to the RANK Protein Structure

(A) Schematic representation of the RANK protein and the mutations found in our patients. The intracellular (In) and extracellular (Out) sides of the membrane (depicted in blue) are represented. Letters and numbers inside the circles indicate the mutated residues. The Y141 inside the square (blue) is a polymorphism not previously described.

(B) Alignment of RANK protein sequences from several species in the regions covering the identified mutations. The mutated residues (red) are indicated above the sequences. The corresponding residues in the individual sequences are also in red. The graphical view of domain structure was obtained by ProtoNet (automatic hierarchical classification of protein sequences).

from Pt. 1A cells. The specificity of the defect for RANKL signaling was confirmed by the fact that TNFα induced normal p38 and ERK1/2 phosphorylation in both control and patient cells (Figure 4D). Sufficient cells from other patients for examination of abnormalities in RANK signaling were unavailable.

Immunological Investigations

Serum immunoglobulin levels were assessed in four out of eight patients and were reduced in three of them (Pt. 1A, Pt. 1B, and Pt. 3; see Table 1). In addition, two of these patients (Pt. 1A and Pt. 3) failed to produce antibodies after a full course of tetanus toxoid vaccination (Table 1).

In *Tnfrsf11a*$^{-/-}$ mutant mice, a developmental defect in the B cell lineage, resulting in a marked reduction of mature B cells in the periphery, has been described.[8] Hence, a detailed immunological analysis was carried out with the peripheral blood obtained from Pt. 1A and Pt. 1B. In particular, we analyzed the following B cell subsets: naive (IgD^+CD27^-), memory (IgD^+CD27^+), and switched-memory (IgD^-CD27^+). Although both patients (tested at 6 and 3 years of age, respectively) had normal proportions of

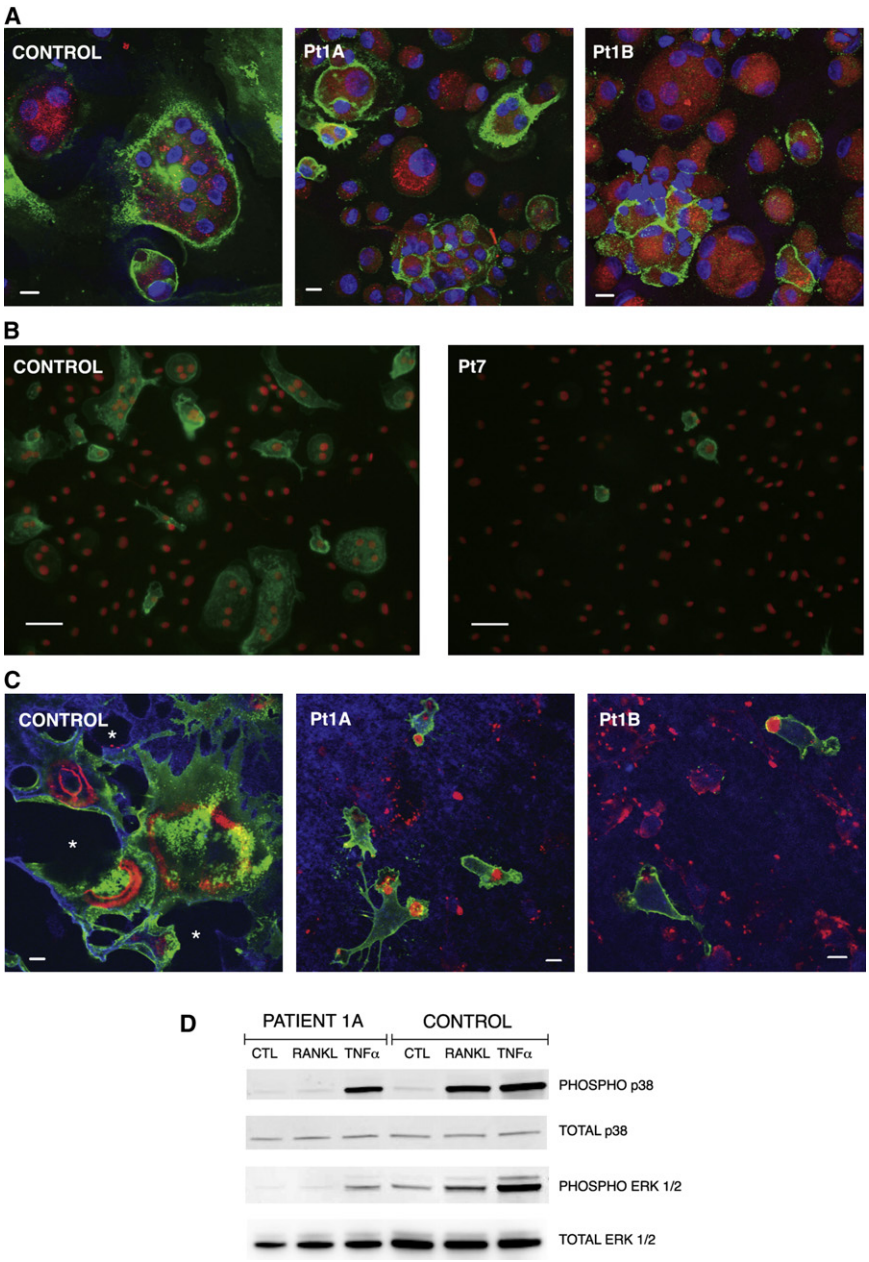

Figure 4. Mutations in *TNFRSF11A* Prevent p38 and ERK1/2 Signaling and Inhibit the Formation of Osteoclasts

(A) Osteoclasts were generated from PBMCs of nontransplanted patients 1A and 1B and one unrelated control (CONTROL), in concurrent cultures. One-micrometer confocal images of cells were cultured on glass coverslips. Osteoclasts were immunostained for αvβ3 (green); acidic vesicles were labeled prior to fixation with lysotracker (red); nuclei were stained with TO-PRO-3 iodide (blue). Multinucleated, αvβ3-positive osteoclasts formed readily in control cultures, whereas in the patient cultures, αvβ3-positive cells were much scarcer and were not multinucleated.

(B) Osteoclasts were generated from PBMCs from nontransplanted Pt. 7 and one of his parents (CONTROL) on tissue-culture plastic. Images were taken with a nonconfocal fluorescent microscope. Osteoclasts are stained for αvβ3 (green), and nuclei are stained with DAPI (pseudocolored red). Clearly, cultures from Pt. 7 do not demonstrate any multinucleated VNR-positive cells, whereas these are abundant in the parent-control culture.

(C) Confocal images (1 μm optical slices) of cultures on dentine discs. Cultures were immunostained for αvβ3 (green), then counterstained with TRITC-phalloidin to visualize osteoclast F-actin (red). The dentine surface was labeled with FL-ALN (blue); dark areas correspond to resorption pits (absence of FL-ALN) and are indicated by asterisks. Actively resorbing osteoclasts formed in the control cultures but not in the cultures from either patient.

Scale bars in panels A and C represent 10 μm. Scale bar in panel B represents 50 μm.

(D) M-CSF-dependent macrophages from Pt. 1A or from a healthy control (CONTROL) were treated for 10 min with RANKL or for 15 min with TNFα. Cell lysates were then analyzed for the presence of phosphorylated and total forms of p38 and ERK1/2. There is an increase in phosphorylation of p38 and ERK1/2 in response to RANKL in the control cells but not in the patient cells, whereas both patient and control respond to TNF by increased phosphorylation of p38 and ERK1/2.

circulating $CD19^+$ B cells, IgD^-CD27^+ B cells were markedly reduced (Figure 5). These cells were present in both *TCIRG1*- and *OSTM1*-deficient patients but absent (as expected) in a HyperIgM patient with a *CD40* defect (MIM 606843). Interestingly, a *TNFSF11*-dependent ARO patient had a normal percentage of these cells when tested at the age of 6 years. Phenotypical and functional analysis of T lymphocytes did not reveal any major abnormalities (data not shown). Because osteoclasts originate from a precursor common to DC lineage, we investigated the in vitro response to IL-4 and GM-CSF of $CD14^+$ monocytes purified from Pt. 1A and Pt. 1B. These cells were able to differentiate into immature DCs, and upon LPS stimulation, they normally upregulated activation markers (CD80, CD86). Moreover, when immature and mature DCs were tested in MLR assays for their priming ability toward allogeneic naive T cells, no defects were observed (Figure 6 and Figure 7). Overall, these data suggest no defects in dendritic function.

Discussion

Mutations in the signal peptide of RANK have been associated with unusual skeletal phenotypes, including familial

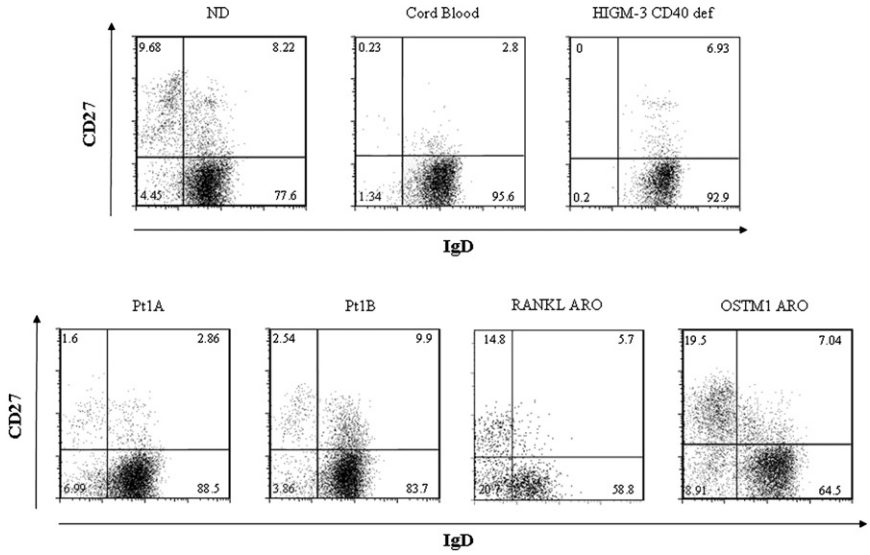

Figure 5. Cytofluorimetric Analysis of Naive and Memory B Cells in Osteoclast-Poor, *TNFRSF11A*-Dependent ARO Patients

FACS analysis of a pediatric normal donor (7 years), a cord-blood sample, a Hyper-IgM-3 patient with *CD40* defect, Pt. 1A (6 years), Pt. 1B (3 years), a *TNFSF11*-dependent ARO patient (6 years), and an *OSTM1*-dependent osteoclast-rich ARO patient (2 years). Mature B cells were then analyzed for IgD and CD27 surface expression.

expansile osteolysis (FEO [MIM 174810]), expansile skeletal hyperphosphatasia, and early-onset Paget disease (PDB [MIM 602080]).[16–18] Here, we report the first example, to our knowledge, of mutations in the human *TNFRSF11A* gene causing a defect in osteoclast formation leading to the clinical findings of osteopetrosis. In our series of seven unrelated families, there were five missense mutations, of which four caused amino acid substitutions in the extracellular domain, one caused amino acid substitutions in the intracellular domain, and two caused stop mutations within the intracellular domain. It is likely that the mutations in the extracellular domain affect the interaction of RANK with RANKL. The complete lack of p38 (MIM 600289) and ERK1/2 signaling through RANK seen in the p.Arg170Gly mutation (Family 1) strongly indicates that the receptor is dysfunctional. The p.Gly280X and p.Trp434X truncating mutations in the intracellular domain cause the loss of a region (^{535}IVVY^{538} in mouse, AA 547–550 in humans) known to be essential for commitment of macrophages to the osteoclast lineage and for ligand-independent oligomerization of RANK,[19,20] as well as the loss of NFκB-activating motifs required for osteoclast formation.[21] However, the effect of the p.Ala244Ser mutation is less clear, because this region of RANK can be deleted without affecting osteoclast formation.[20] Further studies are required to fully understand the effect of each of these mutations in RANK on receptor oligomerization and downstream signaling pathways. Of note, Pt. 1A, Pt. 1B, and Pt. 3 showed immunoglobulin deficiency and Pt. 1A and Pt. 3 also failed to produce antibodies to tetanus toxoid. Analysis of PBMC from both patients from Family 1 suggested that the *TNFRSF11A* mutation is associated with a partial defect in peripheral B cell maturation, given that a reduced number of memory switched cells was found in these patients but not in osteoclast-rich ARO patients. Overall, the defects identified in these patients are compatible with a diagnosis of Common Variable Immune Deficiency (CVID). However, normal serum immunoglobulin levels were reported in Pt. 5, suggesting some variability of the immunological phenotype.

The prevalence of osteoclast-poor osteopetrosis is not easily determined because bone biopsies are rarely performed in ARO patients. In our series of 230 families, we detected six families bearing *TNFSF11* mutations (ref. [6] and unpublished results) and seven families with *TNFRSF11A* abnormalities (this paper). In addition, we have five cases of bone-biopsy-documented osteoclast-poor ARO patients in whom no mutation was found in these genes. This suggests that osteoclast-poor forms contribute to less than 10% of ARO cases and that for about 30% of these, the gene is still unknown.

The exact reasons for the defect in immunoglobulin (Ig) production shown in three patients from two different families are not completely clear. To our knowledge, no data on serum Ig isotype levels was reported for the *Tnfrsf11a*$^{-/-}$ mice. We were able to document impairment in memory B cell populations in the two analyzed brothers. One hypothesis is that RANK could contribute, together with other receptors of the TNFR family, to the process of Ig switch and antibody maturation. Alternatively, the process of antibody response to antigens in these mice could be altered by their defect in the formation of secondary lymphoid tissues. Unfortunately, we were unable to investigate the lymph-node status in our patients because no imaging studies were performed during life and no autopsy was performed at death.

Tnfrsf11a deficiency in mice has also been associated with severe abnormalities in thymic epithelial cells and impaired negative selection, with severe autoimmune manifestations.[22] Therefore, these abnormalities could not be corrected by HSCT. However, none of our patients developed autoimmunity before or after HSCT, possibly indicating a less-critical role for both RANKL and RANK in immune homeostasis in humans.

In the last few years, the molecular dissection of ARO heterogeneity has allowed us to identify at least four

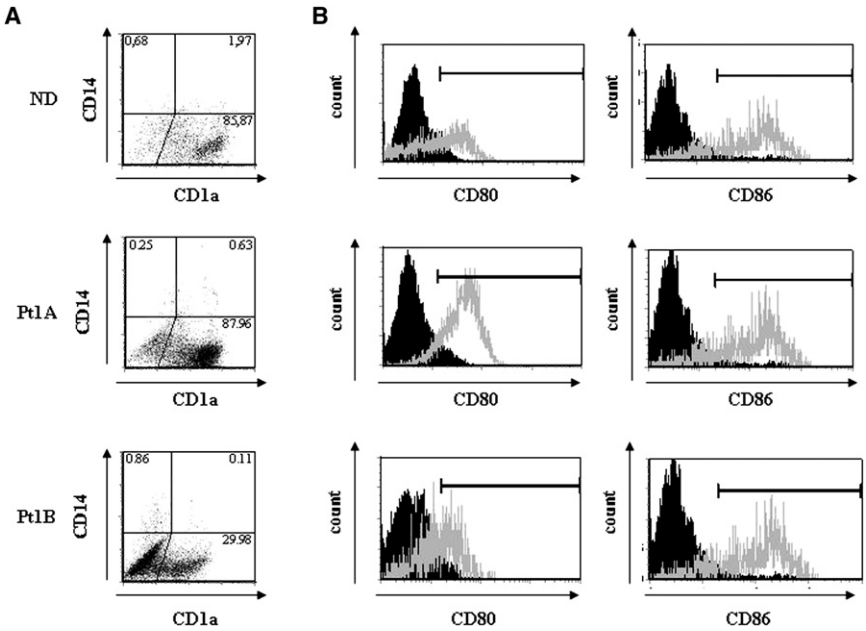

Figure 6. In Vitro Differentiation of Dendritic Cells

(A) DC phenotypes of healthy donor, Pt. 1A, and Pt. 1B were assessed by cytofluorimetric analysis after 6 days of culture of $CD14^+$-enriched monocytes in the presence of GM-CSF and IL-4.

(B) DC maturation in response to 24 hr of LPS exposure was confirmed by the expression of maturation markers (CD80 and CD86). Black-filled histograms represent expression of CD80 and CD86 on non-LPS-stimulated cells, whereas gray-lined empty histograms represent expression on LPS-stimulated cells.

genotypes in the osteoclast-rich form and two subsets in the osteoclast-poor form. The genetic defect could not be characterized in about 25% of patients in our series. However, the molecular defects identified thus far are already of clear clinical and prognostic relevance.[23] Patients with *TNFRSF11A*-deficient ARO share with the *TCIRG1*-dependent ARO patients the classical osteopetrotic phenotype (OPTB1 [MIM 259700]), including secondary neurological symptoms, and both can be cured with HSCT. However, the clinical course of both *TNFRSF11A*-deficient and *TCIRG1*-deficient ARO clearly differs from what is observed in AROs caused by mutations in *OSTM1* (MIM 607649) and, to some extent, *ClCN7* (MIM 602727). Patients with the latter AROs are characterized by rapid and severe primary central nervous system involvement that cannot be rescued by HSCT; thus, additional neurological investigations should be performed prior to the offer of transplantations. The *TNFRSF11A*-dependent form of ARO also differs from the osteoclast-poor *TNFSF11*-dependent form of ARO, which cannot be rescued with HSCT but which is potentially responsive to exogenous-RANKL administration. Although RANK-mediated signaling plays a role in B cell maturation, no obvious immunological defect was identified in the *TNFSF11*-dependent ARO patients that we previously reported.[6] On the contrary, defective immunoglobulin production in three patients with *TNFRSF11A*-defective ARO, together with the documented impairment of B cell maturation in the two patients tested at the cellular level, suggests that, at variance with mice, mutations in the receptor or its ligand have different effects on the development of the immune system in humans. Additional studies are needed in order to clarify whether other, *TNFSF11*-independent, signaling pathways are responsible for this difference. Overall, these results highlight the clinical importance of the molecular diagnosis of genetic diseases of bone.

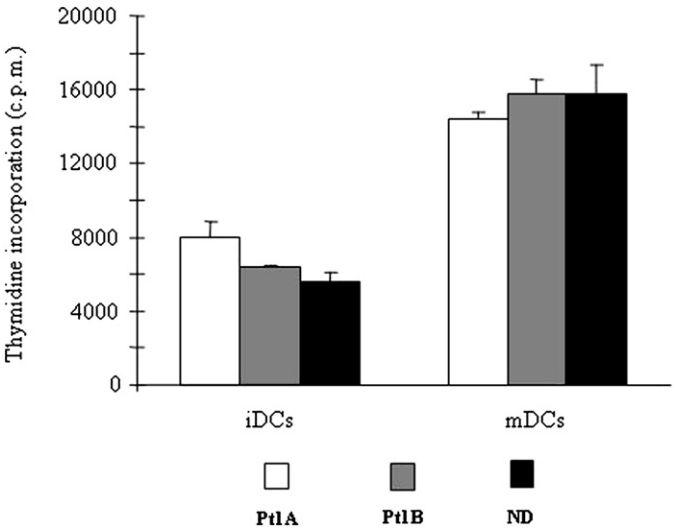

Figure 7. Mixed Lymphocyte Reaction

5×10^3 $CD1a^+CD14^-$ cells, immature DCs, and mature DCs were cultured with 5×10^4 $CD4^+CD45RA^+$ naive allogenic T lymphocytes, purified from healthy-donor peripheral blood. Proliferative responses were assessed by ^{3}[H] thymidine incorporation after 72 hr of coculture, after a 16 hr pulse with 1 μ Ci/well ^{3}[H] thymidine. Vertical bars indicate standard errors calculated over three replicates.

Supplemental Data

One table and one figure are available at http://www.ajhg.org/.

Acknowledgments

This work was supported by grants from Eurostells (STELLAR) and FIRB/MIUR to P.V. (RBIN04CHXT), from the Fondazione Telethon to C.S. (grant GGP08176), from the Fondazione Cariplo to A.F and from ISS Malattie Rare (New cell therapy approaches for infantile malignant Osteopetrosis) to P.V. and E-rare project to A.V.. The work reported in this paper has also been funded by the N.O.B.E.L. (Network Operativo per la Biomedicina di Eccellenza in Lombardia) Program from Fondazione Cariplo to P.V. and A.V. and by the European Calcified Tissue Society (M.H.H.) and the Chief Scientist's Office of the Scottish Executive, grant CZB/4/495 (M.H.H. and F.P.C.). The technical assistance of Maria Elena Caldana, Dario Strina, Lucia Susani and Kevin Mackenzie is acknowledged. We thank Jemni Ben Chibani and Ahmed-Noureddine Helal for providing DNA from normal individuals.

Received: April 15, 2008
Revised: June 6, 2008
Accepted: June 16, 2008
Published online: July 10, 2008

Web Resources

The URLs for data presented herein are as follows:

Online Mendelian Inheritance in Man (OMIM), http://www.ncbi.nlm.nih.gov/Omim/
ProtoNet, http://www.protonet.cs.huji.ac.il

References

1. Tolar, J., Teitelbaum, S.L., and Orchard, P.J. (2004). Osteopetrosis. N. Engl. J. Med. *351*, 2839–2849.
2. Frattini, F., Orchard, P.J., Sobacchi, C., Giliani, S., Abinun, M., Mattsson, J.P., Keeling, D.J., Andersson, A.K., Wallbrandt, P., Zecca, L., et al. (2000). Defects in the TCIRG1-encoded 116kD subunit of the vacuolar proton pump are responsible for a subset of human autosomal recessive osteopetrosis. Nat. Genet. *25*, 343–346.
3. Kornak, U., Kasper, D., Bösl, M.R., Kaiser, E., Schweizer, M., Schulz, A., Friedrich, W., Delling, G., and Jentsch, T.J. (2001). Loss of the ClC-7 chloride channel leads to osteopetrosis in mice and man. Cell *104*, 205–215.
4. Chalhoub, N., Benachenhou, N., Rajapurohitam, V., Pata, M., Ferron, M., Frattini, A., Villa, A., and Vacher, J. (2003). Grey-lethal mutation induces severe malignant autosomal recessive osteopetrosis in mouse and human. Nat. Med. *9*, 399–406.
5. Van Wesenbeeck, L., Odgren, P.R., Coxon, F.P., Frattini, A., Moens, P., Perdu, B., MacKay, C.A., Van Hul, E., Timmermans, J.P., Vanhoenacker, F., et al. (2007). Involvement of PLEKHM1 in osteoclastic vesicular transport and osteopetrosis in incisors absent rats and humans. J. Clin. Invest. *117*, 919–930.
6. Sobacchi, C., Frattini, A., Guerrini, M.M., Abinun, M., Pangrazio, A., Susani, L., Bredius, R., Mancini, G., Cant, A., Bishop, N., et al. (2007). Osteoclast-poor human osteopetrosis due to mutations in the gene encoding RANKL. Nat. Genet. *39*, 960–962.
7. Döffinger, R., Smahi, A., Bessia, C., Geissmann, F., Feinberg, J., Durandy, A., Bodemer, C., Kenwrick, S., Dupuis-Girod, S., Blanche, S., et al. (2001). X-linked anhidrotic ectodermal dysplasia with immunodeficiency is caused by impaired NF-kappa-B signaling. Nat. Genet. *27*, 277–285.
8. Dougall, W.C., Glaccum, M., Charrier, K., Rohrbach, K., Brasel, K., De Smedt, T., Daro, E., Smith, J., Tometsko, M.E., Maliszewski, C.R., et al. (1999). RANK is essential for osteoclast and lymph node development. Genes Dev. *13*, 2412–2414.
9. Kong, Y.Y., Yoshida, H., Sarosi, I., Tan, H.L., Timms, E., Capparelli, C., Morony, S., Oliveira-dos-Santos, A.J., Van, G., Itie, A., et al. (1999). OPGL is a key regulator of osteoclastogenesis, lymphocyte development and lymphnode organogenesis. Nature *397*, 315–323.
10. Kim, N., Odgren, P.R., Kim, D.K., Marks, S.C. Jr., and Choi, Y. (2000). Diverse roles of the tumor necrosis factor family member TRANCE in skeletal physiology revealed by TRANCE deficiency and partial rescue by a lymphocyte-expressed TRANCE transgene. Proc. Natl. Acad. Sci. USA *97*, 10905–10910.
11. Kim, D., Mebius, R.E., MacMicking, J.D., Jung, S., Cupedo, T., Castellanos, Y., Rho, J., Wong, B.R., Josien, R., Kim, N., et al. (2000). Regulation of peripheral lymph node genesis by the tumor necrosis factor family member TRANCE. J. Exp. Med. *192*, 1467–1478.
12. Taylor, A., Rogers, M.J., Tosh, D., and Coxon, F.P. (2007). A novel method for efficient generation of transfected human osteoclasts. Calcif. Tissue Int. *80*, 132–136.
13. Blair, H.C., Borysenko, C.W., Villa, A., Schlesinger, P.H., Kalla, S.E., Yaroslavskiy, B.B., Garćia-Palacios, V., Oakley, J.I., and Orchard, P.J. (2004). In vitro differentiation of CD14 cells from osteopetrotic subjects: contrasting phenotypes with TCIRG1, CLCN7, and attachment defects. J. Bone Miner. Res. *19*, 1329–1338.
14. Collins, J.S., and Schwartz, C.E. (2002). Detecting polymorphisms and mutations in candidate genes. Am. J. Hum. Genet. *71*, 1251–1252.
15. Asagiri, M., and Takayanagi, H. (2007). The molecular understanding of osteoclast differentiation. Bone *40*, 251–264.
16. Hughes, A.E., Ralston, S.H., Marken, J., Bell, C., MacPherson, H., Wallace, R.G., van Hul, W., Whyte, M.P., Nakatsuka, K., Hovy, L., et al. (2000). Mutations in TNFRSF11A, affecting the signal peptide of RANK, cause familial expansile osteolysis. Nat. Genet. *24*, 45–48.
17. Whyte, M.P., and Hughes, A.E. (2002). Expansile skeletal hyperphosphatasia is caused by a 15-base pair tandem duplication in TNFRSF11A encoding RANK and is allelic to familial expansile osteolysis. J. Bone Miner. Res. *17*, 26–29.
18. Nakatsuka, K., Nishizawa, Y., and Ralston, S.H. (2003). Phenotypic characterization of early onset Paget's disease of bone caused by a 27-bp duplication in the TNFRSF11A gene. J. Bone Miner. Res. *18*, 1381–1385.
19. Xu, D., Wang, S., Liu, W., Liu, J., and Feng, X. (2006). A novel receptor activator of NF-kappaB (RANK) cytoplasmic motif plays an essential role in osteoclastogenesis by committing macrophages to the osteoclast lineage. J. Biol. Chem. *281*, 4678–4690.
20. Kanazawa, K., and Kudo, A. (2005). Self-assembled RANK induces osteoclastogenesis ligand-independently. J. Bone Miner. Res. *20*, 2053–2060.
21. Liu, W., Xu, D., Yang, H., Xu, H., Shi, Z., Cao, X., Takeshita, S., Liu, J., Teale, M., and Feng, X. (2004). Functional identification of three receptor activator of NF-kappa B cytoplasmic

motifs mediating osteoclast differentiation and function. J. Biol. Chem. *279*, 54759–54769.

22. Rossi, S.W., Kim, M.Y., Leibbrandt, A., Parnell, S.M., Jenkinson, W.E., Glanville, S.H., McConnell, F.M., Scott, H.S., Penninger, J.M., Jenkinson, E.J., et al. (2007). RANK signals from CD4(+)3(-) inducer cells regulate development of Aire-expressing epithelial cells in the thymic medulla. J. Exp. Med. *204*, 1267–1272.
23. Frattini, A., Vezzoni, P., Villa, A., and Sobacchi, C. (2007). The Dissection of Human Autosomal Recessive Osteopetrosis Identifies an Osteoclast-Poor Form due to RANKL Deficiency. Cell Cycle *6*, 3027–3033.